La-promoted Ni-hydrotalcite-derived catalysts for dry reforming of methane at low temperatures

Hongrui Liu, Dominik Wierzbicki, Radoslaw Debek, Monika Motak, Teresa Grzybek, Patrick da Costa, Maria Elena Gálvez

La-promoted Ni-hydrotalcite-derived catalysts for dry reforming of methane at low temperatures

Hongrui Liu [a], Dominik Wierzbicki[b], Radoslaw Debek[a,b], Monika Motak[b], Teresa Grzybek[b], Patrick Da Costa[a] *, Maria Elena Gálvez[a]

[a] Sorbonne Universités, UPMC, Univ. Paris 6, CNRS, UMR 7190, Institut Jean Le Rond d'Alembert, 2 place de la gare de ceinture, 78210 Saint-Cyr-L'Ecole, France

[b] AGH University of Science and Technology, Faculty of Energy and Fuels, Al. A. Mickiewicza 30, 30-059 Cracow, Poland

*Corresponding author. Tel: +33-1-30854865; fax: + 33-1-30854899,

patrick.da_costa@*upmc.fr*

Abstract

La-promoted Ni-containing hydrotalcite-derived catalysts were prepared and tested in dry methane reforming at low-moderate temperatures. The prepared materials were characterized by means of X-ray diffraction (XRD), temperature programmed reduction (H_2-TPR) and CO_2-temperature programmed desorption (TPD). The presence of lanthanum was found to enhance the reforming reaction, but also direct methane decomposition at low reaction temperatures. This fact was assigned to an increased presence of Ni^0 sites as a consequence of improved reducibility of Ni-species in the La-promoted catalysts. Lanthanum can well contribute to the gasification of amorphous carbon deposits, resulting in lower overall carbon deposition at 550°C.

Keywords: Dry methane reforming, syngas, hydrogen production, nickel catalysts, lanthanum, hydrotalcites.

1. Introduction

Dry reforming of methane (DRM), the reforming of methane with CO_2: $CH_4(g)+ CO_2(g) = 2CO(g) + 2H_2(g)$, ΔH_0 (298K)= +247 kJ·mol^{-1}, is nowadays considered as a perspective alternative for the production of syngas, H_2 + CO, involving the valorization of CO_2, coming either from capture or naturally present in the reactant gas, i.e. such in biogas. Furthermore, the H_2/CO molar ratio in DRM-syngas, equal to 1, makes it applicable for Fischer-Tropsch synthesis [1-4]. There are, however, several important drawbacks that hinder the practical application of DRM, such as its high endothermicity, and different issues related to the selectivity and stability of the DRM catalyst under operation conditions [5,6]. The co-existence of parallel reactions, such as direct methane decomposition and the reverse water gas shift reaction results in low yields and in catalyst deactivation through carbon deposition, especially at low reaction temperatures. Increasing the temperature favors DRM thermodynamics, but Ni particles tend to sinter leading to a dramatic decrease in the catalytic performance.

Different active metals, e.g. Ru, Pt, Pd, Ni or Rh, supported on different materials, have been proposed as DRM catalysts [7-12, 19]. Among them, nickel shows comparable activity to noble metals, being much cheaper and more readily available. Current research efforts focus on finding support materials and promoters that improve the selectivity of the process and that contribute to enhanced catalytic stability. As an example, Verykios [20] showed that the incorporation of Ni onto La_2O_3 support notably improved the catalysts stability in comparison to Ni-Al_2O_3, through the formation of oxy-carbonate species ($La_2O_2CO_3$) that were further able to gasify the already formed carbon deposits.

Also known as layered double hydroxides, hydrotalcites are mixed hydroxide materials having the general formula: $[M_{1-x}^{II}M_x^{III}(OH)_2][A_{x/n}^{n-}] \cdot mH_2O$, where M^{II} / M^{III}

represent divalent and trivalent metal ions and A^{n-} hydrated anion. Their composition can be easily modified through the substitution of different divalent and trivalent cations in the brucite layers, i.e. substituting Mg^{2+} by Ni^{2+}. The works of Cavani et al. show that even monovalent and tetravalent cations such as Li^{+}, Zr^{4+}, Ti^{4+} and Sn^{4+} can be as well introduced into these hydrotalcite-layers [21]. Therefore, the acid-base and redox properties of hydrotalcite-derived oxides can be properly tailored to fit any particular catalytic application [22, 23]. Moreover, the materials obtained after calcination of the hydrotalcite matrix offer other interesting properties, such as adequate porosity, and a random and homogeneous distribution of the different cations on the resulting mixed-oxide structure. As a consequence, Ni-containing hydrotacite-derived materials have been recently considered as promising catalysts for DRM [18, 24-26].

The addition of promoters can positively influence activity, selectivity and/or stability of hydrotalcite-derived catalysts. Among them, the incorporation of rare earth oxides can help controlling DRM selectivity, through the inhibition of carbon formation reactions, or strengthened CO_2 adsorption on the support [26-29]. Debek et al. [26, 30] found that incorporation of Ce into Ni-containing hydrotalcite-derived catalysts resulted in an increased reducibility of nickel species, and led to the formation of new strong basic sites, which improved the long-term stability of these catalysts in DRM reaction. However, CO_2 and CH_4 conversion became somewhat lower. Lanthanum has also been considered as a promoter of Ni-containing hydrotalcite-derived catalysts for DRM. Previous published papers just evidence the promotion effect of La, or its promoting effect in combination with noble metals or other promoters [18, 31, 32]. Serrano-Lotina et al. [31] studied the influence of calcination temperature on the activity of a Ni (2.3 wt.%) catalyst containing La (1.3 wt.%). Lucredio et al. [32] prepared several hydrotalcite-derived catalysts containing 10 wt.% of Ni and 10 wt.% of La and/or 1 wt.% of Rh. La-promotion did not lead to improvement of activity but

increased the stability in the DRM reaction. It should be taken into account that the activity of Ni-containing hydrotalcite-derived catalysts strongly depends on the amount of Ni-cations introduced in the pristine hydrotalcite structure [33]. The best performance was observed for the catalysts containing ca. 20 wt.% of Ni (i.e. 25 % of exchanged Mg in the catalysts). There is still no clear understanding of the effect of lanthanum incorporated to hydrotalcites containing a constant amount of nickel. Moreover, so far and to the best of our knowledge, only the work of Yu and co-workers takes into consideration the incorporation of different amounts of La, however, La-loadings employed (3-10 wt.%) were much higher than the ones used in the preparation of the catalysts presented herein.

Thus, the present works considers the addition of lanthanum (1-4 wt.%) to 15 wt.% Ni-containing hydrotalcite-derived catalysts for dry reforming of methane. Special attention has been paid to the influence of La-promotion on the physico-chemical properties of the hydrotalcite-derived catalysts, as studied by means of XRD, H_2 TPR and CO_2 TPD, and its consequences in terms of activity, selectivity and stability in the DRM reaction.

2. Experimental

2.1 Synthesis of the hydrotalcite-derived catalysts

Hydrotalcites containing M(III) trivalent and M(II) divalent metals (Al, La, Mg, Ni,) with M(III)/M(II) molar ratio of 0.33, were prepared by a co-precipitation method at constant pH (from 9.5 to 10). Two aqueous solutions, one containing the mixed nitrates of divalent and trivalent metals, and a second one containing sodium hydroxide (1M), were added dropwise into a flask containing an aqueous solution of sodium carbonate, and subsequently kept under vigorous stirring at 65°C and constant pH. This mixture aged for 24h and then filtered, carefully washed with deionized water and finally dried overnight at 80°C. The nominal (assumed) concentration of the different components in each hydrotacite prepared (un-promoted and La-promoted), as well as their labeling, is listed in Table 1. In order to obtain the corresponding hydrotalcite-derived catalysts, each hydrotalcite was calcined under air at 550°C for 4 hours.

2.2 Physico-chemical characterizaion

X-ray diffraction (XRD) patterns were acquired in a PANalytical-Empyrean diffractometer, equipped with CuK_α ($\lambda = 1.5406$ Å) radiation source, within 2θ range from 3 to 90°, with a step size of 0.02°/min. The Scherrer equation was used for calculating the Ni crystal size on the reduced HT-derived catalyts. Temperature programmed reduction (H_2-TPR) profiles were obtained in a BELCAT-M (BEL Japan) device, equipped with a thermal conductivity detector (TCD). The calcined hydrotalcites were first outgassed at 100°C for 2h and then reduced using 5% vol. H_2-Ar at a heating rate of 7.5°C/min, from 100 °C to 900 °C. Temperature programmed desorption (CO_2-TPD) was performed using the same apparatus (BELCAT-M). The catalysts were first degassed for 2 h at 500°C and then cooled to 80°C. Subsequently, a mixture of 10% vol. CO_2-He was fed for 1h in order to saturate their surface

with CO_2, followed by the desorption of weakly (physically) adsorbed CO_2 under a flow of pure He for 15 minutes. Then, the catalysts were heated up from 80°C to 900°C under He, at 10°C/min and the evolution of CO_2 was followed with the aid of a TCD detector. The amount of carbon deposited on the surface of each catalysts upon the DRM reaction was measured by means of its thermogravimetric oxidation in a SDT Q600 apparatus (TA Instruments), under air flow (100 mL/min), heating from ambient temperature to 900°C at a rate of 10°C/min. The resulting materials were grinded and sieved keeping the solid fraction corresponding to a particle size distribution between 100-300 μm.

2.3 Dry reforming of methane (DRM) activity tests

The activity of the different HT-derived catalysts was assayed in an experimental set-up consisting of a tubular quartz reactor (8 mm internal diameter) heated inside the catalytic fixed bed was measured with the aid of a K-type thermocouple. A series of mass-flow meters (Brooks) allowed the fed of 100 mL/min of a reactant mixture containing $CH_4/CO_2/Ar$ in a volume ratio 1/1/8, corresponding to a GHSV of 20,000h^{-1}. Prior to each DRM experiment, each HT-derived catalysts was reduced in situ at 900°C for 1h under a 5% vol. H_2-Ar mixture. Upon reduction the catalytic bed was cooled down to 850°C and the reactant gas mixture was supplied to the reactor. The catalytic activity was then followed from 850°C to 550°C, at 30 minutes of steady-state interval. The concentration of the different products contained in the gas exiting the catalytic reactor were analyzed online using Varian GC4900 micro chromatograph equipped with a TCD detector. CO_2 and methane conversions as well as the H_2/CO ratios were calculated as follows, where n_i^{in} and n_i^{out} are the concentrations of each species entering and exiting the reactor:

$$X_{CO_2} = \frac{\left(n_{CO_2}^{in} - n_{CO_2}^{out}\right)}{n_{CO_2}^{in}} \times 100 \qquad \text{(eq. 1)}$$

$$X_{CH_4} = \left(n^{in}_{CH_4} - n^{out}_{CH_4}\right) \Big/ n^{in}_{CH_4} \times 100 \qquad\qquad \text{(eq. 2)}$$

$$H_2/CO = n^{out}_{H_2} / n^{out}_{CO} \qquad\qquad \text{(eq. 3)}$$

The thermodynamic equilibrium composition of the system was calculated through the minimization of Gibbs free energy. Equations 1, 2 and 3 were as well used for calculating the thermodynamic limits in terms of CH_4, CO_2 conversions and H_2/CO ratio.

3. Results and discussion

3.1 Physico-chemical properties of the non-promoted and La-promoted hydrotalcite-derived catalysts

3.1.1 Reducibility of Ni-species

Figure 1 a shows the H_2-TPR profiles for the HT-derived catalysts after calcination. All prepared catalysts exhibit one wide asymmetric peak (820-850°C) arising from the reduction of Ni-oxide species to Ni°. Such Ni-oxide species are most probably inserted into the Al-Mg mixed oxide matrix resulting from the calcination of the hydrotalcite brucite layers, forming a solid solution of high thermal stability [18,30]. The presence of lanthanum modifies the reducibility of the Ni-species in these HT-derived catalysts. The main reduction peak shifts to lower temperatures with increasing La-content, i.e. from 850 °C for HN4, non-promoted, to 830 °C and 820°C for the La-promoted catalysts. Additionally, a shoulder can be observed at ca. 690°C for the La-promoted catalysts HN2 and HN3 (2 and 4 wt.% of La, respectively), which can be assigned to segregated NiO species, pointing to weaker Ni-support interaction as a consequence of the incorporation of lanthanum [13, 18, 31, 32]. In the case of HN2, two wide additional peaks can be clearly observed at about 400 and 450°C, pointing to the presence of bulk weakly-bonded NiO. Moreover, Yu and co-workers concluded that the presence of lanthanum positively influenced the dispersion of these NiO

species, since such low temperature peaks were shifted to slightly higher reduction temperatures, pointing to smaller crystal sizes upon an increase in the La-content [34].

The segregation of Ni-species during reduction, as well as the reducibility of the segregated NiO species were further confirmed by H_2-TPR experiments performed on the HT-derived catalysts reduced at 900°C for 1 h under 5% vol. H_2/Ar. The results of these experiments are shown in Figure 1 b. ~~First of all, it seems that the reduction treatment was not efficient enough to reduce all the Ni present in the HT-derived catalysts, since some H_2 was still consumed during these TPR experiments.~~ A single reduction peak appears now at much lower temperatures, i.e. at 230°C for HN1 and HN4 (low La-content and non-promoted catalyst), at 247°C for HN2 (2% wt. La) and at 254°C for HN3 (4% wt. La), pointing to Ni or NiO segregation from the Mg-Al mixed oxide structure during this reduction treatment [35], and corresponding to the reduction temperatures typically reported for bulk NiO [35, 36]. The exposure to ambient air of the readily reduced catalysts may have caused the reoxidation of a part of this segregated Ni-species. The integration of each peak allows the quantification of the presence of such bulk NiO species on each catalyst. The results are presented in Table 2. Hydrogen consumption during the TPR experiments performed on the reduced catalysts is higher for both the non-promoted catalysts, HN4, and the catalyst containing the highest amount of La, HN3, i.e. 0,529 mmol H_2/g and 0.602 mmol H_2/g, respectively. This points to an increased presence of reluctant NiO species upon the reduction treatment for HN4 and HN3. On the contrary, lower La content leads to a decrease in H_2 consumption, that becomes minimal in the case of the HT-derived catalyst promoted with 2% wt. of La, HN2, i.e. 0,438 mmol H_2/g. Lower H_2 consumption points to a reduced presence of remaining NiO species and, thus, to a higher availability of reduced Ni^0 sites, moreover indicating that there is an optimal La-loading in terms of reducibility of Ni-species.

3.1.2 Crystallinity: La-segregation and Ni crystal size

The X-ray diffractograms for the fresh hydrotalcites, the HT-derived catalysts before and after reduction are shown in Figure 2 a, b and c. The diffraction patterns acquired for the fresh hydrotalcites, Fig. 2 a, evidence the typical reflections and a layered hydrotalcite phase at $2\theta = 11°$, $24°$ and $35°$, respectively corresponding to (003), (006) and (009) planes, confirming the existence of a multilayer structure [35]. The hydrotalcite containing the highest amount of La (HN3) showed the presence of additional $La_2(CO_3)_2(OH)_2$ and $La_2O_2CO_3$ phases, as seen in Fig. 2 a. The absence of other phases in these patterns, points to the successful incorporation of nickel into the hydrotalcite structure.

The unit cell parameters were calculated using the method proposed by Rives [36] and are summarized in Table 2. The parameter c was calculated from the positions of the three first reflections $c = d_{(003)} + 2d_{(006)} + 3d_{(009)}$. This parameter is thus indicative of the distance between brucite layers in the hydrotalcite structure, which strongly depends on the type and orientation of the interlayer anions [16]. The parameter a of the unit cell, which describes the average distance between cation-cation in brucite layers, was calculated from the position of the first reflection at $2\theta = 60°$. Parameter a remains unchanged upon La-loading, suggesting that La was not incorporated into the interlayer space of the hydrotalcite structure. On the contrary, a large increase in this a unit cell distance would have been observed due to the larger ionic radius of La in comparison with Mg and Al ions [34].

After calcination, Fig. 2b, XRD patterns evidence three reflections at $2\theta = 43.5$ and $63°$ characteristic of the periclase-like structure of mixed oxides generated upon the thermal decomposition of hydrotalcite materials. In the case of the La-containing HT-derived catalysts, some reflections corresponding to a segregated La_2O_3 phase can be observed,

together with some residual La carbonates that might be formed upon exposition of the calcined materials to ambient air conditions.

The XRD patterns recorded for the reduced catalysts, Fig. 2 c, conserve the characteristic of the mixed oxide periclase structure. Moreover, additional phases can be observed corresponding to metallic nickel, i.e. $2\theta = 44.5°$, $54°$ and $78°$, and segregated La_2O_3. Crystal sizes calculated for the metallic Ni phase range from 6.3 and 8.9 nm. No clear influence of La-promotion on crystal size can be observed.

3.1.3 Influence of La-promotion on catalyst basicity

The TPD profiles registered for the according to literature [29,35,37-39], there are three typical CO_2 desorption peaks normally appearing in CO_2-TPD profiles for hydrotalcite-derived materials, appearing between 100 and 500°C. These peaks are representative of the presence of basic sites having different strength: weak Brønsted basic sites such as surface OH groups (low temperature), medium-strength Lewis acid-base sites (intermediate temperature), and low-coordination oxygen anions acting as strong basic sites (high temperature). In fact, these three contributions are clearly visible in the CO_2-TPD profiles acquired for the different HT-derived catalysts, shown in Figure 3. However, mean peak positions and its areas change as a consequence of the presence of La and with La-loading.

Table 3 contains a listing of the temperatures corresponding to each peak's maximal intensity, as well as the results of its deconvolution and integration (area = µmol CO_2 desorbed per gram of catalyst). In general, the three CO_2 desorption peaks for La-promoted catalysts occur respectively at 133-139°C, 232-246°C and 353-370°C, while in the case of the non-promoted catalyst they appear centered at 147°C, 250°C and 389°, i.e. at much higher temperatures, pointing to weaker CO_2 chemisorption as a consequence of the presence of La. This is particularly true for HN2, i.e. the HT-derived catalysts containing 2% wt. La, since the

first and the second peak, corresponding to weak and medium-strength basicity, appear 14 and 11°C earlier than for the non-promoted catalyst, HN4.

Total basicity, i.e. the total area under the three peaks, increases for HN2 and HN3. The maximal amount of CO_2 desorbed corresponds however to HN2, pointing to 2% wt as the optimal La-loading in terms of catalyst basicity. Moreover, upon the introduction of 2% wt. La, the presence of medium-strenght basic sites (Lewis pairs) seems to be exceptionally boosted. Upon 4% wt. La-loading, HN3, weak basic sites seems to be as well promoted.

3.2 Dry reforming of methane (DRM) experiments: influence of La-promotion

3.2.1 Catalytic activity and selectivity

Figure 4 a and b shows the CH_4 and CO_2 conversions measured during the DRM experiments in the presence of the different HT-derived catalysts, as a function of reaction temperature. The results obtained within the low temperature window, i.e. 550 and 600°C, are shown in detail in the inset contained in each figure.

As expected, both CH_4 and CO_2 conversions increase with increasing temperature for any of the catalysts tested and independently of the La-content, in agreement with the trend forecasted by thermodynamics. However, especially at low temperatures, some differences can be observed that are worth to be remarked. First of all, at 550 and 600°C, CO_2 conversions measured are all the times slightly higher than CH_4 conversions, whereas the opposite trend is predicted by thermodynamics, i.e. at 550°C, for HN2 36% CH_4 and 33% CO_2 conversion is measured while the thermodynamically predicted conversions are 87% and 42% for CH_4 and CO_2, respectively. Direct methane decomposition reaction, as well as the Bouduard reactions – among other carbon forming reactions – are generally thermodynamically favored reaction at such low temperatures, but they do not seem to be completely activated in the presence of this series of catalysts. Other reactions, such as the water gas shift reaction may contribute to enhanced CO_2 conversion. As a consequence, the H_2/CO ratios experimentally measured, shown in Figure 5, considerably apart from the high values 3.5-2 predicted by the thermodynamics in the low temperature window, 550°C-600°C. And it is precisely within this range of temperatures that very clear differences are observed among the non-promoted and the La-promoted catalysts.

Moreover, La-content influences the activity and selectivity of these HT-derived catalysts. The lowest methane conversions are all the time measured for the non-promoted

catalyst, which, at the same time, does not seem to be very active towards CO_2 conversion. The presence of La boosts the activity of the catalyst. As a consequence, HN2, containing 2% wt. La, shows the highest activities of this series at 550°C in terms of both CH_4 and CO_2 conversion, whereas HN3, containing 4% wt. La, is the most active catalyst at 600°C. However, at low temperatures, the thermodynamic prevalence of methane decomposition with respect to the reverse water gas shift reaction leads to a stronger promotion of the former vis-à-vis the later, above all in the presence of a Ni-containing catalyst [41]. Moreover, the increased presence of available Ni^0 sites in HN2 and HN3, pointed out by their physico-chemical characterization, may explain such higher activities, since it is well know that, kinetically, the limiting step for both reforming and methane decomposition reaction is the activation of the C-H bond, taking place on metallic Ni sites [42]. At the lowest reaction temperature, i.e. 550°C, the promotion of direct methane decomposition is consequently reflected in the values of the H_2/CO molar ratio obtained, Fig. 5, which increase with increasing catalytic activity for the La-promoted HT-derived catalysts. The decreasing H_2/CO values measured for HN3 at temperatures from 550 to 650°C may point to increased selectivity towards the dry reforming of methane (DRM) and/or the reverse water-gas shift (RWGS) reactions at 650°C for this La-promoted catalysts, as has been previously reported in literature [19]. The increased presence of weak basic sites in this catalyst containing 4% wt. La, may result in a weak-type of interaction between CO_2 and the support, leading to the promotion of DRM and RWGS, once the temperature is sufficiently high to overcome their thermodynamic barriers.

Other authors have previously studied the behavior of Ni-containing hydrotalcite-derived catalysts in DRM. [20, 21, 30-34]. Dębek et al. [30] evaluated the promoting effect of Ce and Zr in the low temperature DRM behavior of Ni-containing Mg/Al or Al hydrotalcites, under the same experimental conditions used in our present work. The presence of either Ce

13

or Zr resulted in increased stability of the catalysts. Ce was found to partially avoid methane decomposition and enhance the oxidation of the carbon deposits, whereas Zr strongly modified the selectivity of the DRM reaction set. Concerning the influence of La as promoter, the comparison of our results to previously published studies is not straight forward, since the experimental conditions are not quite similar, both for the pretreatment of the catalysts (calcination and reduction temperatures) and DRM activity tests. This is a crucial issue, since the calcination and reduction temperature plays an important role in the final catalytic activity, as shown by Serrano et al. [31]. However, it can be generally stated that La addition results in an improved stability. Serrano et al. [31] confirmed this fact during DRM experiments performed at 700°C on Ni (2.3 wt.%) Mg/Al hydrotalcite-derived catalysts promoted with 1.3 wt.% La. Yu et al. [34] also studied the activity of Ni-containing hydrotalcite-derived catalysts promoted with different La contents (3-10 wt.%) at 600-800°C. The addition of lanthanum increased the CO_2 adsorption ability, the amount of surface Ni and significantly improved the stability of these catalysts.

3.2.2 Catalytic stability: carbon formation and evolution of Ni crystal sizes

The HT-derived catalysts after DRM testing were analyzed by means of X-ray diffraction. The obtained patterns are shown in Figure 6. Some additional phases are now present in the spent catalysts that were not observed in the diffractograms shown previously in Figure 2, i.e. representative of the presence of graphite and of the formation of the alloy $MgNi_3$. The formation of this $MgNi_3$ implies the reduction of Mg^{2+} cations. This may be however possible at relatively high temperatures and under carbothermal reduction conditions, i.e. in the presence of methane and C [43]. Graphite formation is due to carbon formation reactions, mainly direct methane decomposition. Ni^0 crystal sizes were recalculated for the

spent catalysts. The values are shown in Table 2. A considerable reduction of crystal size takes place during DRM, since the Ni^0 crystal size after test are much smaller than those calculated for the reduced catalysts, i.e. it changes from 8.4 nm to 4.5 nm in the reduced and spent HN3 catalyst, respectively. During reaction a redistribution of Ni^0 particles takes place, probably due to the formation of isolated Ni-species that are continuously extracted from the Ni-Mg-Al mixed oxide matrix and reduced under DRM reaction atmosphere.

Isothermal DRM experiments were conducted at 550°C on HN4 and HN3 catalysts, i.e. the non-promoted and 4% wt. La-promoted HT-derived catalysts. Figure 7 shows the CH_4 and CO_2 conversions, as well as the H_2/CO ratio, measured over more than 8 hours time-on-stream (TOS). An estimation of the rate of C formation, in µg/min – estimated from the carbon balance, is plotted together with CH_4 conversion in Figure 7a. The activity and selectivity of both HN4 and HN3 change with time on stream. This means that the evolution of the catalytic system continues even after 8 hours TOS, and that further longer-duration experiments need to be performed in order to further conclude on catalytic stability. In any case, either La-promoted or not, the values of H_2/CO ratio increases as the isothermal experiment progresses. This can be assigned to the creation of new and readily reduced Ni^0 species of smaller crystal size, active in direct methane decomposition yielding C(s) and H_2, which is thermodynamically favored at such low temperatures. In agreement with the enhanced reducibility of Ni-species, this fact becomes especially true for the La-promoted catalyst, HN3. In consequence carbon formation rate is as well higher all the time for HN3 than for the non-promoted catalyst, HN4.

The extent of carbon formation was evaluated by means of thermogravimetric oxidation of HN4 and HN3 after the isothermal DRM experiments. Figure 8 a and b shows the thermogravimetric curves – weight loss and its derivative as a function of temperature – obtained for these two catalysts. Slightly higher amount of carbon is formed during DRM at

550°C in the presence of the non-promoted catalyst, HN4. <u>The comparison of the amount of carbon deposited calculated from the thermogravimetric curves and the integration of the carbon balance show an interesting mismatch, i.e. 12.6 mg of deposited C according to TGA vs. 30.5 that should be theoretically present of the spent HN3 catalyst after reaction, according to the carbon balance.</u> The presence of La may favor the formation of lanthanum oxycarbonates, able to gasify the carbon deposits, and above all the non-crystalline amorphous carbon formed during reaction [20]. In fact, the derivative, dTGA, is substantially different for HN3 (La-promoted), than for HN4 (unpromoted), pointing to the presence of different relative amounts of amorphous and graphitic carbon. The dTGA peak can be deconvoluted into two Gaussian contributions: a first peak, appearing at temperatures higher than 450°C, due to the oxidation of "coating" or amorphous carbon, and a second one, centered at about 600-650°C, corresponding to the oxidation of filamentous carbon formed through methane direct decomposition on Ni-sites [44]. The low-temperature peak assigned to the presence of amorphous carbon has a lower contribution to the oxidation profile and appears shifted to higher reaction temperatures. The gasification of such amorphous carbon deposits in the presence of lanthanum oxycarbonate species may have contributed to this fact. Moreover, the high-temperature peak corresponding to carbon filaments and fibers grown on Ni-sites is clearly marked in the La-promoted catalyst, HN3, in agreement with the increased presence of Ni^0 species and its evolution with time-on-stream leading to the enhancement of direct methane decomposition reaction.

4. Conclusions

La-promoted Ni-containing HT-derived catalysts were prepared from MgAl hydrotalcites and tested in methane dry reforming at temperatures from 550°C to 850°C. The physico-chemical characterization of these materials evidenced bulk NiO segregation and

enhanced Ni-reducibility for the La-promoted catalysts. Medium strength and weak basicity were found to be boosted in such La-containing catalyst, depending on La-loading.

Mostly as a consequence of the increased presence of reduced Ni^0 sites, the activity of the La-promoted catalysts was found to be higher than for the non-promoted HT-derived catalyst. However, the presence of La results as well in the promotion of undesirable side reactions, such as direct methane decomposition, thermodynamically favorable at low temperatures, i.e. 550°C. In spite of this, La can contribute to the gasification of amorphous carbon deposits, through the formation of oxycarbonate species, thus resulting in overall lower carbon formation during long-duration isothermal experiments performed at 550°C.

References

[1] G. Centi, S. Perathoner, Opportunities and prospects in the chemical recycling of carbon dioxide to fuels. Catalysis Today, 2009 ;148 ; 191-205.

[2] J.H. Edwards, A.M. Maitra, The chemistry of methane reforming with carbon dioxide and its current and potential applications, Fuel Processing Technology, 1995 ; 42 ;269-289.

[3] A.S. Al-Fatesh, M.A. Naeem, A.H. Fakeeha, A.E. Abasaeed, CO_2 reforming of methane to produce syngas over γ-Al_2O_3 supported Ni-Sr catalysts, Bulletin of the Chemical Society Japan, 2013 ; 86 ;742-746.

[4] M.C.J. Bradford, M.A. Vannice, Catalytic reforming of methane with carbon dioxide over nickel catalysts II. Reaction kinetics, Applied Catalysis A: General, 1996 ;142 ;97-122.

[5] K.Y. Koo, S.H. Lee, U.H. Jung, H.S. Roh, W.L. Yoon, Syngas production via combined steam and carbon dioxide reforming of methane over Ni-Ce/MgAl$_2$O$_4$ catalysts with enhanced coke resistance, Fuel Processing Technology, 2014 ;119 ;151-157.

[6] M.M. Barroso-Quiroga, A.E. Castro-Luna, Catalytic activity and effect of modifiers on Ni-based catalysts for the dry reforming of methane, International Journal of Hydrogen Energy, 2010 ;35 ;6052-6056

[7] M.F. Mark, W.F. Maier. CO$_2$-Reforming of Methane on Supported Rh and Ir Catalysts. Journal of Catalysis,1996;164:122–130.

[8] V. Yu Bychkov, O.V. Krylov, V.N. Korchak, Kinet. The Mechanistic Study of Methane Reforming with Carbon Dioxide on Ni/α-Al$_2$O$_3$. Kinetics and Catalysis. 2002; 43: 86–94.

[9] A.N.J. van Keulen, K. Seshan, J.H.B.J. Hoebink, J.R.H. Ross. TAP Investigations of the CO$_2$ Reforming of CH$_4$ over Pt/ZrO$_2$. Journal of Catalysis., 1997;166:306–314.

[10] V.C.H. Kroll, H.M. Swaan, S. Lacombe, C. Mirodatos. Methane Reforming Reaction with Carbon Dioxide over Ni/SiO$_2$ Catalyst: II. A Mechanistic Study Journal of Catalysis, 1998; 164: 387–398.

[11] J.L. Pinilla, I. Suelves, M.J. Lázaro, R. Moliner, J.M. Palacios. Influence of nickel crystal domain size on the behaviour of Ni and NiCu catalysts for the methane decomposition reaction. Applied Catalysis A: General, 2009; 363: 199-207.

[12] A. Serrano-Lotina, A.J. Martin, M.A. Folgado, L. Daza, Dry reforming of methane to syngas over La-promoted hydrotalcite clay-derived catalysts, International Journal of Hydrogen Energy, 2012 ;35 ;12342-12350.

[13] J.-H. Kima, D.J. Suhb, T.J. Park, K.-L. Kima. Effect of metal particle size on coking during CO$_2$ reforming of CH$_4$ over Ni–alumina aerogel catalysts. Applied Catalsis A: General, 2000; 197: 191–200.

[14] Sutthiumporn K, Kawi S. Promotional effect of alkaline earth over Ni-La$_2$O$_3$ catalyst for CO$_2$ reforming of CH$_4$: Role of surface oxygen species on H2 production and carbon suppression. International Journal of Hydrogen Energy, 2011; 36:14435-14446.

[15] Pompeo F, Gazzoli D, Nichio NN. Stability improvements of Ni/α-Al$_2$O$_3$ catalysts to obtain hydrogen from methane reforming. International Journal of Hydrogen Energy, 2009; 34:2260-2268.

[16] Sun NN, Wen X, Wang F, et al. Catalytic performance and characterization of Ni-CaO-ZrO$_2$ catalysts for dry reforming of methane. Applied Surface Science, 2011; 257: 9169-9176.

[17] Gao J, Hou ZY, Guo JZ, et al. Catalytic conversion of methane and CO$_2$ to synthesis gas over a La$_2$O$_3$-modified SiO$_2$ supported Ni catalyst in fluidized-bed reactor. Catalysis Today, 2008; 131: 278-284.

[18] A. Serrano-Lotina, L. Rodríguez, G. Muñoz, L. Daza, Biogas reforming on La-promoted NiMgAl catalysts derived from hydrotalcite-like precursors, Journal of Power Sources, 2011 ; 196 :4404-4410.

[19] A. Albarazi, P. Beaunier, P. Da Costa, International Journal of Hydrogen Energy, 2013 ; 38 :127–139.

[20] X. Verykios, Catalytic dry reforming of natural gas for the production of chemicals and hydrogen, International Journal of Hydrogen Energy, 2003 ;28 ; 1045-1063.

[21] F. Cavani, F. Trifiro, A. Vaccari, Hydrotalcite-type anionic clays : Preparation, properties and applications, Catalysis Today, 1991 ;11 ;173-302.

[22] C.C. Forano, U. Prevot, V. Taviot Gueho, C. In, F. Bergaya, B.K.G. Theng, G. Lagaly, Handbook of Clay Science, Elsevier Ltd., UK, 2013, pp. 745.

[23] D.P. Debecker, E.M. Gaigneaux, G. Busca, Exploring, tuning, and exploiting the basicity of hydrotalcites for applications in heterogeneous catalysis, Chemistry-A European Journal, 2009; 15: 3920-3935.

[24] C.E. Daza, S. Moreno, R. Molina, Ce-incorporation in mixed oxides obtained by the self-combustion method for the preparation of high performance catalysts for the CO_2 reforming of methane, Catalysis Communications, 2010 ;12 :173-179.

[25] C.E. Daza, C.R. Cabrera, S. Moreno, R. Molina, Syngas production from CO_2 reforming of methane using Ce-doped Ni-catalysts obtained from hydrotalcites by reconstruction method, Applied Catalysis A: General, 2010 ; 378 :125-133.

[26] R. Dębek, M.E. Galvez, F. Launay, M. Motak, T. Grzybek, P. Da Costa, Low temperature dry methane reforming over Ce, Zr and CeZr promoted Ni-Mg-Al hydrotalcite-derived catalysts, International Journal of Hydrogen Energy, 2016; in press.

[27] Gao J, Hou ZY, Guo JZ, et al. Catalytic conversion of methane and CO_2 to synthesis gas over a La_2O_3-modified SiO_2 supported Ni catalyst in fluidized-bed reactor. Catalysis Today, 2008; 131: 278-284.

[28] J. Zhu, X. Peng, L. Yao, J. Shen, D. Tong, C. Hu, The promoting effect of La, Mg, Co and Zn on the activity and stability of Ni/SiO2 catalyst for CO2 reforming of methane, International Journal of Hydrogen Energy, 2011 ; 36 : 7094-7104.

[29] M.-S. Fan, A.Z. Abdullah, S. Bhatia, Catalytic Technology for Carbon Dioxide Reforming of Methane to Synthesis Gas, ChemCatChem, 2009 ;1 ;192-208.

[30] R. Dębek, M. Radlik, M. Motak, M. E. Galvez, W. Turek, P. Da Costa, T. Grzybek, Ni-containing Ce-promoted hydrotalcite derived materials as catalysts for methane reforming with carbon dioxide at low temperature – On the effect of basicity, Catalysis Today, 2015 ; 257 : 59-65

[31] A. Serrano-Lotina, L. Rodriquez, G. Munoz, A.J. Martin, M.A. Folgado, L. Daza, Biogas reforming over La-NiMgAl catalysts derived from hydrotalcite-like structure: Influence of calcination temperature, Cat. Comm., 12 (2011) 961-967.

[32] A. Lucredio, J.M. Assaf, E.M. Assaf, Reforming of a model sulfur-free biogas on Ni catalysts supported on Mg(Al)O derived from hydrotalcite precursors : Effect of La and Rh addition, Biomass and Bioenergy, 2014 ; 60 ;8-17.

[33] R. Dębek, M. Adamowska, M. Motak, P. Da Costa, T. Grzybek, Hydrotalcite derived catalysts with different Ni/Mg/Al molar ratios as a catalyst for low temperature dry reforming of methane, conference materials: GC-P-05, 8th International Conference on Environmental Catalysis, 24-27.08.2014, Asheville, NC, USA

[34] X. Yu, N. Wang, W. Chu, M. Liu, Carbon dioxide reforming of methane for syngas production over La-promoted NiMgAl catalysts derived from hydrotalcites, Chemical Engineering Journal, 2012 ;209 :623–632.

[33] C. Li, Y.W. Chen, Temperature-programmed reduction studies of nickel oxide/alumina catalysts: effects of the preparation method, Thermochimica Acta, 1995 ; 256: 457-564

[34] B. Mile, D. Stirling, M.A. Zammitt, A. Lovell, M. Webb, The location of nickel oxide and nickel in silica-supported catalysts : Two form of NiO and the assignment of temperature-programmed reduction profiles, Journal of Catalysis, 1988 ;114 :217-229.

[35] O.D. Pavel, D. Tichit, I.C. Marcu, Acido-basic and catalytic properties of transition-metal containing Mg-Al hydrotalcites and their corresponding mixed oxides, Applied Clay Science, 2012 ;61 : 52-58.

[36] V. Rives, Characterisation of layered double hydroxides and their decomposition products, Materials Chemistry and Physics, 2002 ;75 ; 19-25.

[37] J.I. Di Cosimo, V.K. Diez, M. Xu, E. Iglesia, C.R. Apesteguia, Structure and Surface and Catalytic Properties of Mg-Al Basic Oxides, Journal of Catalysis, 1998 ;178 ; 499-510.

[38] J.I. Di Cosimo, C.R. Apesteguia, M.J.L. Gines, E. Iglesia, Structural Requirements and Reaction Pathways in Condensation Reactions of Alcohols on MgyAlOx Catalysts, Journal of Catalysis, 2000; 190: 261-275.

[39] P. Liu, M. Derchi, E.J.M. Hensen, Promotional effect of transition metal doping on the basicity and activity of calcined hydrotalcite catalysts for glycerol carbonate synthesis, Applied Catalysis B: Environmental, 2014; 144: 135-143.

[40] B.S. Liu, C.T. Au, Carbon deposition and catalyst stability over La_2NiO_4/γ-Al_2O_3 during CO_2 reforming of methane to syngas, Applied Catalysis A: General, 2013; 244: 181–195

[41] Liu Z, Zhou J, Cao K, Yang W, Gao H, Wang Y, et al. Highly dispersed nickel loaded on mesoporous silica: one-spot synthesis strategy and high performance as catalysts for methane reforming with carbon dioxide. Applied Catalysis B: Environmental, 2012; 125: 324–330.

[41] H.F. Abbas, W.M.A.W. Daud, Hydrogen production by methane decomposition: A review, International Journal of Hydrogen Energy, 2010; 35: 1160-1190.

[42] J. Wei, E. Iglesia, Isotopic and kinetic assessment of the mechanism of reactions of CH_4 with CO_2 or H_2O to form synthesis gas and carbon on nickel catalysts, Journal of Catalysis, 2004; 224: 370-383.

[43] M.E. Galvez, A. Frei, G. Albisetti, G. Lunardi, A. SteinfeldSolar hydrogen production via a two-step thermochemical process based on MgO/Mg redox reactions—thermodynamic and kinetic analyses. International Journal of Hydrogen Energy, 2008, 33: 2880-2890.

[44] B.D. Gould, X. Chen, J.W. Schwank, n-Dodecane reforming over nickel-based monolith catalysts: Deactivation and carbon decomposition, Applied Catalysis A: General, 2008; 334: 277-290.

Captions to Figures

Figure 1. H_2-TPR profiles of a) calcined b) reduced HT-derived catalysts.

Figure 2. X-ray diffractograms acquired for a) the fresh hydrotalcites, and the HT-derived catalysts b) before and c) after reduction.

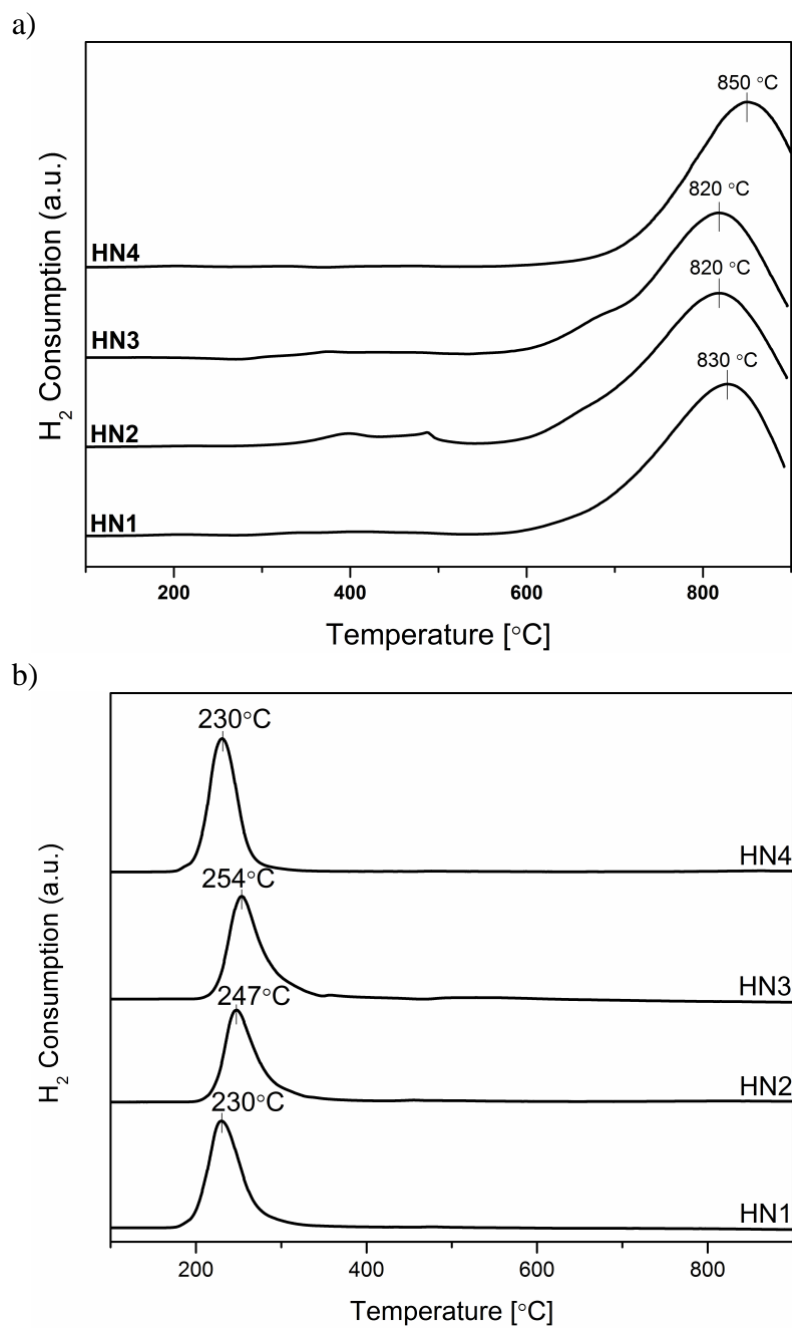Figure 3. CO_2-TPD profiles for the HT-derived reduced catalysts.

Figure 4. DMR experiments: a) CH_4 and b) CO_2 conversions as function of reaction temperature. Inset: zoom of the results obtained at 550 and 600°C. Solid line: thermodynamic equilibrium conversions.

Figure 5. H_2/CO molar ratio versus reaction temperature for the different HT-derived catalysts. Solid line: thermodynamic equilibrium H_2/CO ratio.

Figure 6. X-ray diffractograms for the HT-derived catalysts after the DMR activity test.

Figure 7. Isothermal DMR experiments at 550°C: a) CH_4 and b) CO_2 conversions, c) H_2/CO ratio, vs. time on stream, for HN3 and HN4.
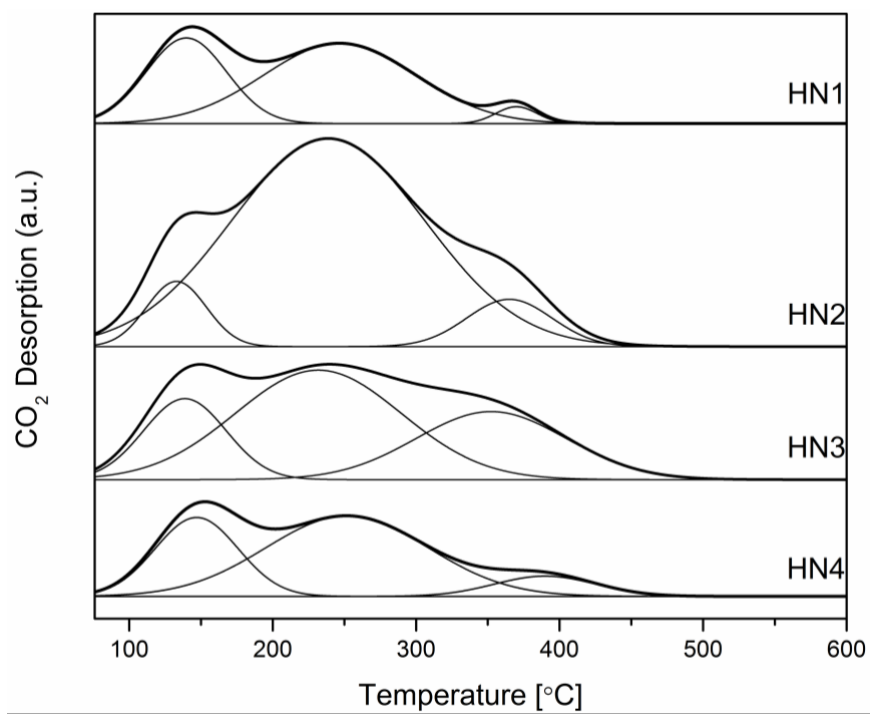
Figure 8. Thermogravimetric oxidation of carbon deposits, weight loss and its derivative for a) HN4 and b) HN3 after DRM.
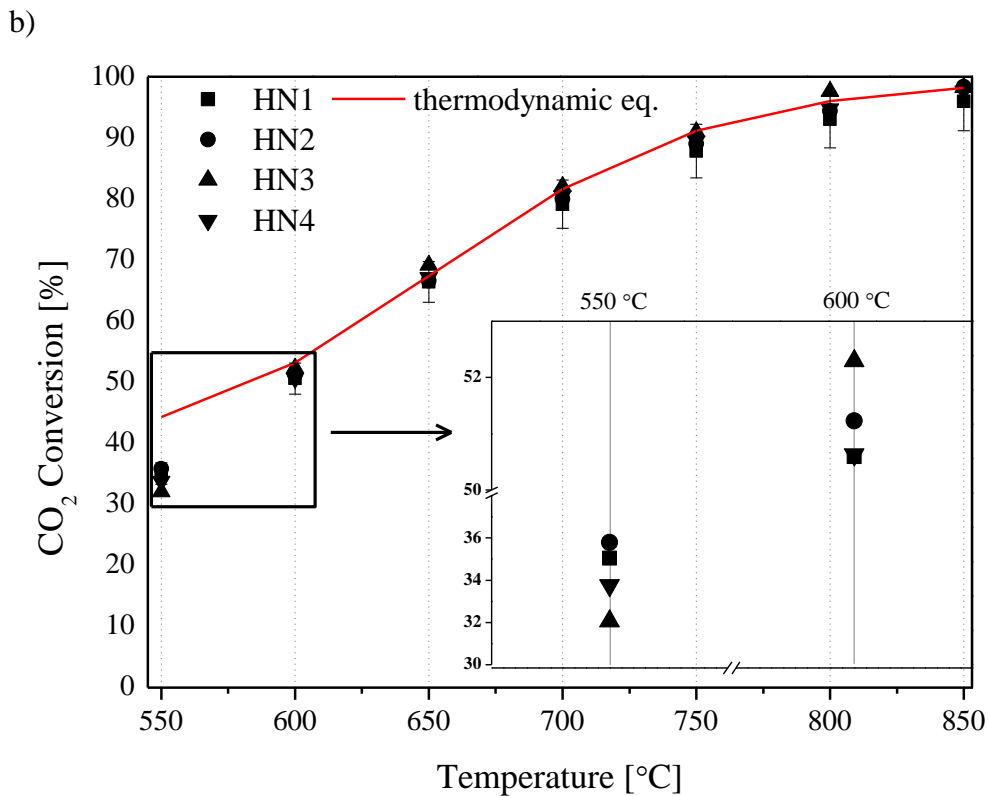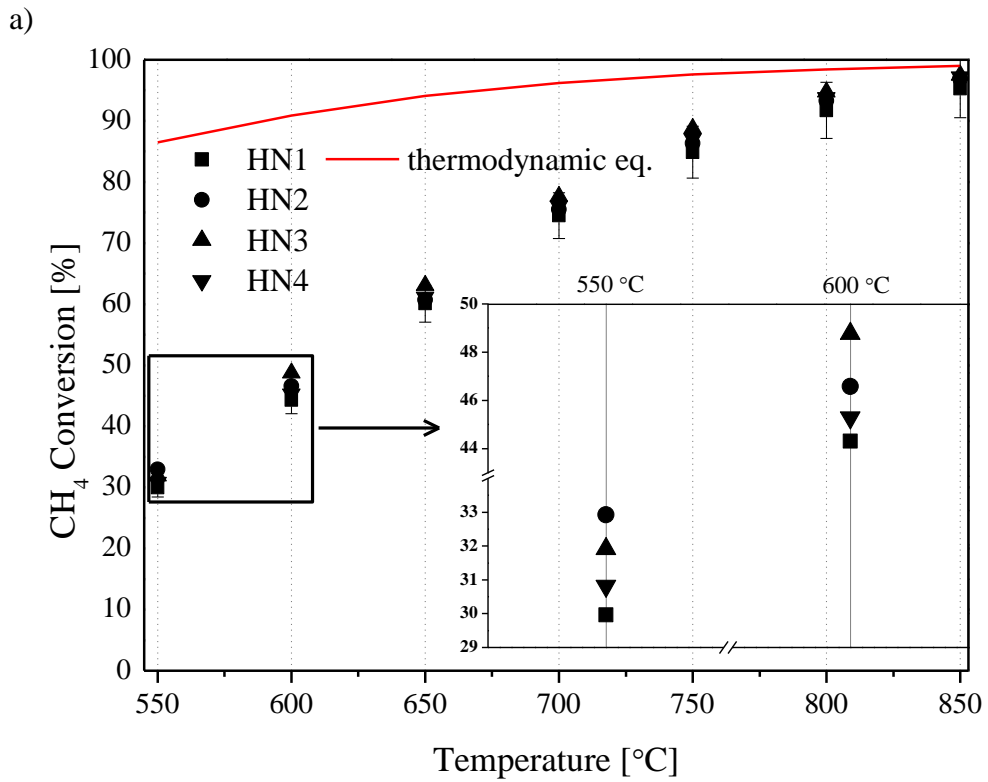
Figure 1. H$_2$-TPR profiles of a) calcined b) reduced HT-derived catalysts.
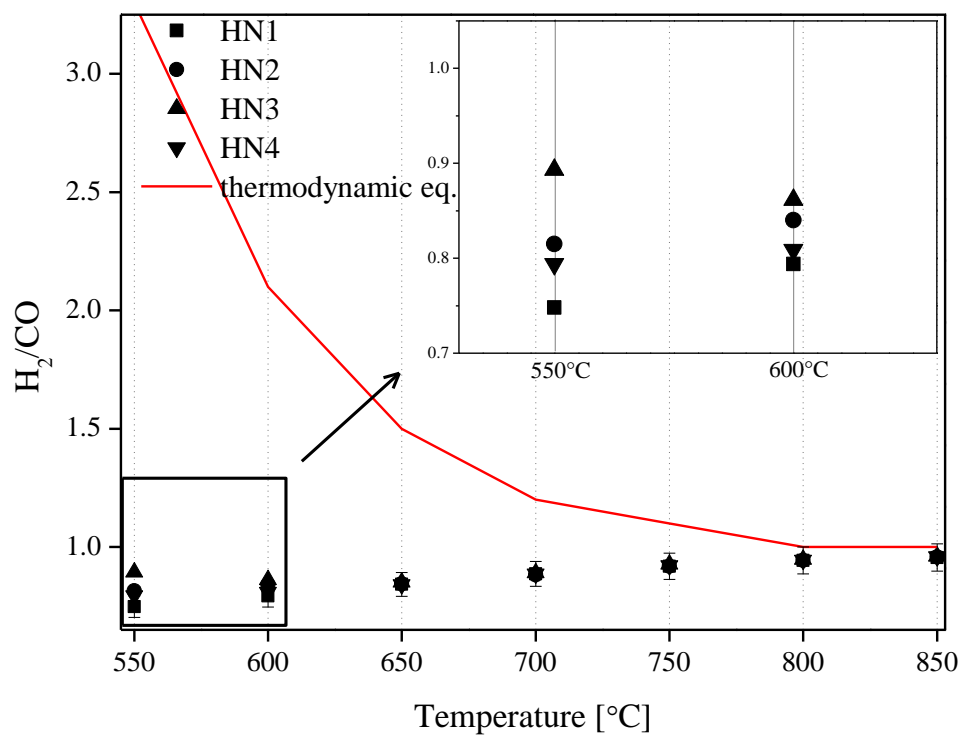
Figure 2. X-ray diffractograms acquired for a) the fresh hydrotalcites, and the HT-derived catalysts b) before and c) after reduction.
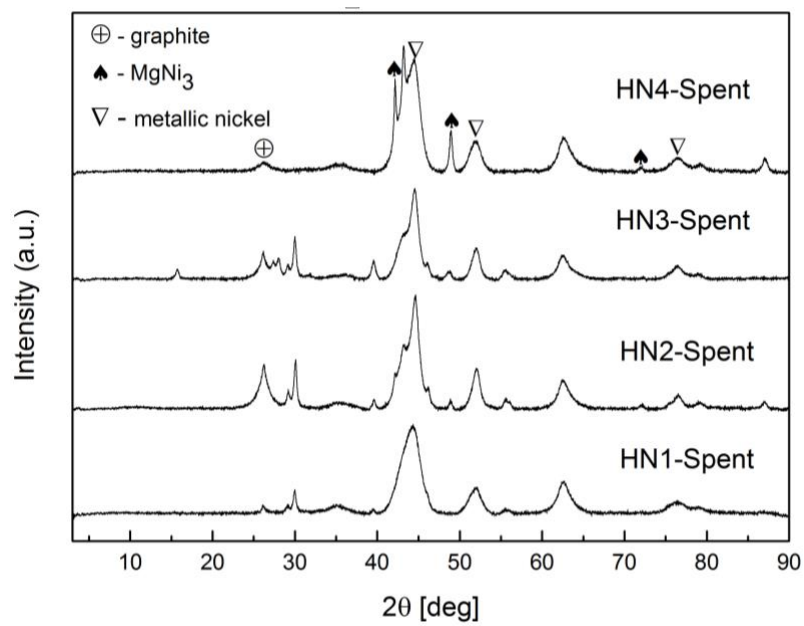
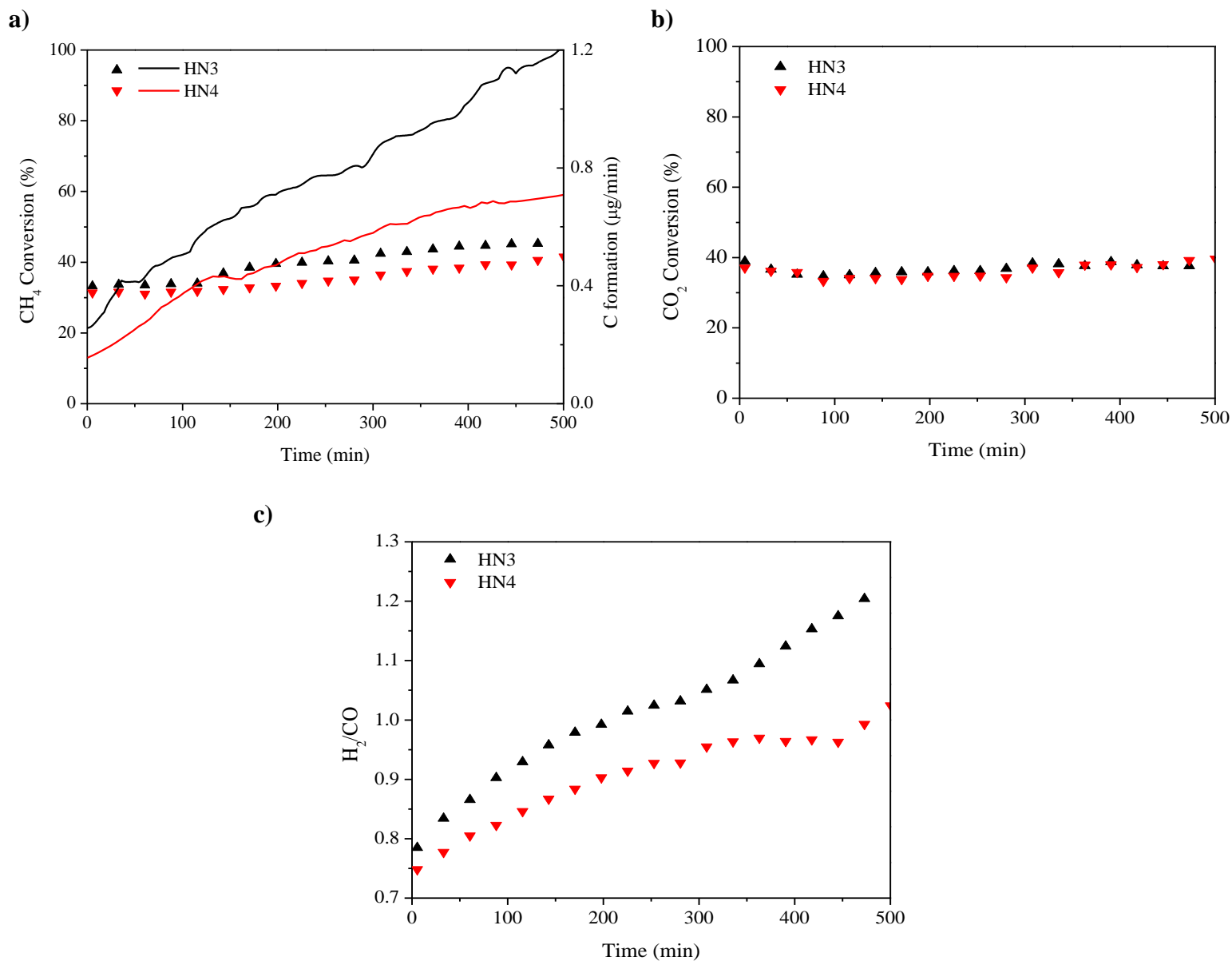**Figure 3. CO₂-TPD profiles for the HT-derived reduced catalysts.**

Figure 4. DMR experiments: a) CH$_4$ and b) CO$_2$ conversions as function of reaction temperature. Inset: zoom of the results obtained at 550 and 600°C. Solid line: thermodynamic equilibrium conversions.

Figure 5. H₂/CO molar ratio versus reaction temperature for the different HT-derived catalysts. Solid line: thermodynamic equilibrium H₂/CO ratio.

Figure 6. X-ray diffractograms for the HT-derived catalysts after the DMR activity test.

a)

b)

c)

Figure 7. Isothermal DMR experiments at 550°C: a) CH$_4$ conversion and C formation calculated from carbon balance, b) CO$_2$ conversion, and c) H$_2$/CO ratio, vs. time on stream, for HN3 and HN4.
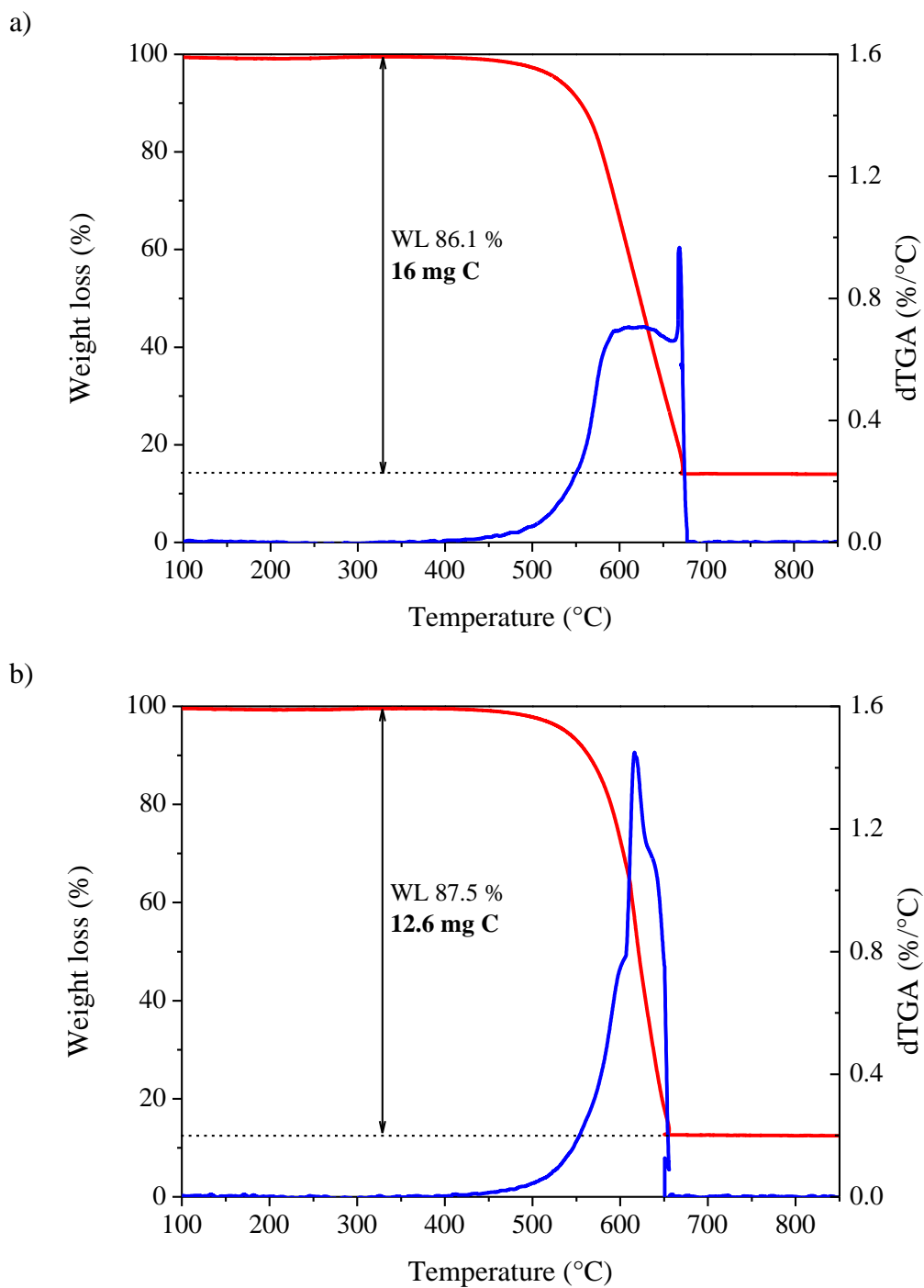
a)

b)

Figure 8. Thermogravimetric oxidation of carbon deposits, weight loss and its derivative for a) HN4 and b) HN3 after DRM.

Table 1. Ni-containing, La-promoted (Me = Ni, La)

$[Me_yMg_xAl_{0.25}(OH)_2](CO_3^{2-})_{0.125} \cdot 0.5H_2O$ hydrotalcites and derived catalysts: Nominal

concentration of the different cations

Hydrotalcite	Catalyst	Metal content [wt.%]				La/Al ratio	$\dfrac{M(III)}{M(II) + M(III)}$
		Ni	La	Mg	Al		
$Ni_{0.215}La_{0.006}Mg_{0.535}Al_{0.244}$	HN1	15	1	15.6	7.9	0,03	0.25
$Ni_{0.215}La_{0.012}Mg_{0.535}Al_{0.238}$	HN2	15	2	15.4	7.6	0,05	0.25
$Ni_{0.22}La_{0.025}Mg_{0.53}Al_{0.225}$	HN3	15	4	15.0	7.1	0,11	0,25
$Ni_{0.21}Mg_{0.54}Al_{0.25}$	HN4	15	0	15.8	8.1	0	0,25

Table 2. H$_2$ consumption for the reduced catalysts, a and b unit cell parameters and Ni crystal size calculated for the HT-derived catalysts (before and after DMR test).

Catalyst	H$_2$ consumption – reduced catalysts (mmol H$_2$/g)	a [Å]	c [Å]	Crystal size [nm]	
				Reduced	Spent
HN1	0.471	3.06	23.43	6.3	4.0
HN2	0.438	3.06	23.49	8.9	4.5
HN3	0.602	3.06	23.52	8.4	4.5
HN4	0.529	3.06	23.46	8.3	3.5